

# Assessing Ionospheric Scintillation Risk for Direct-to-Cellular Communications using Frequency-Scaled GNSS Observations

**Abdollah Masoud Darya**, Graduate Student Member, IEEE  
SAASST, University of Sharjah, Sharjah, UAE

**Muhammad Mubashir Shaikh**  
Electrical Engineering Dept., University of Sharjah, Sharjah, UAE  
SAASST, University of Sharjah, Sharjah, UAE

**Abstract**— One of the key issues facing Direct-to-Cellular (D2C) satellite communication systems is ionospheric scintillation on the uplink and downlink, which can significantly degrade link quality. This work investigates the spatial and temporal characteristics of amplitude scintillation at D2C frequencies by scaling L-band scintillation observations from Global Navigation Satellite Systems (GNSS) receivers to bands relevant to D2C operation, including the low-band, and 3GPP's N255 and N256. These observations are then compared to scaled radio-occultation scintillation observations from the FORMOSAT-7/COSMIC-2 (F7/C2) mission, which can be used in regions that do not possess ground-based scintillation monitoring stations. As a proof of concept, five years of ground-based GNSS scintillation data from Sharjah, United Arab Emirates, together with two years of F7/C2 observations over the same region, corresponding to the ascending phase of Solar Cycle 25, are analyzed. Both space-based and ground-based observations indicate a pronounced diurnal scintillation peak between 20–22 local time, particularly during the equinoxes, with occurrence rates increasing with solar activity. Ground-based observations also reveal a strong azimuth dependence, with most scintillation events occurring on southward satellite links. The scintillation occurrence rate at the low-band is more than twice that observed at N255 and N256, highlighting the increased robustness of higher D2C bands to ionospheric scintillation. These results demonstrate how GNSS scintillation observations can be leveraged to characterize and anticipate scintillation-induced D2C link impairments, which help in D2C system design and the implementation of scintillation mitigation strategies.

(Corresponding author: Abdollah Masoud Darya)

Abdollah Masoud Darya is with SAASST, University of Sharjah, Sharjah, UAE (e-mail: abdollah.masoud@ieee.org). Muhammad Mubashir Shaikh is with the Electrical Engineering Department, College of Engineering, University of Sharjah, Sharjah, UAE (e-mail: mshaikh@sharjah.ac.ae) and with SAASST, University of Sharjah, Sharjah, UAE.

This work has been submitted to the IEEE for possible publication. Copyright may be transferred without notice, after which this version may no longer be accessible.

0018-9251 © IEEE

## I. INTRODUCTION

ONE of the key pillars of the sixth generation (6G) communications paradigm is ubiquitous connectivity [1]. The idea of being connected everywhere at all times is difficult to realize by terrestrial-bound base-stations. Yet, the recent emergence of the *Direct-to-Cellular* (D2C) approach, where standard cellular phones can connect directly to satellites, and vice versa, aims to address this issue [2].

As satellite signals propagate between the transmitter and ground receiver, they are affected by natural propagation effects or artificial sources of interference that reduce the quality of service. The fluctuation of the amplitude and phase of radio waves (*scintillation*) due to the signal's propagation through the ionosphere is one of these sources [3]. Scintillations can occur naturally through interactions between the signal and ionospheric electron-density irregularities [4], or they can be caused by external interfering signals [5]. Ionospheric scintillation significantly attenuates signals under 3 GHz [6], and varies based on several spatial and temporal parameters, such as geographical location, time of day, season, and solar cycle progression.

Global Navigation Satellite Systems (GNSS)-based applications have long faced the issue of scintillation, and their effects on accuracy, availability, and integrity, especially at equatorial and high latitude regions [7]. Even so, the effect on D2C communications systems would be more prominent. This is due to the two-way nature of D2C, with standard users being a part of both uplink and downlink, compared to only downlink for standard GNSS users. Additionally, GNSS is broadcast-based and is resilient to short-term temporal fluctuations due to the usage of tracking techniques [8]. However, D2C communications, especially voice or broadband connectivity, are sensitive to abrupt signal fluctuations.

To better understand the risk of ionospheric scintillation on D2C, dedicated scintillation monitoring stations have to be installed, and long observation campaigns must be performed to study how the scintillation varies with the 11-year solar cycle. This is not feasible, especially since D2C deployment has already begun by some companies [9]. Therefore, this work proposes an alternative.

Ground-based GNSS ionospheric scintillation monitoring stations have long been established to monitor ionospheric irregularities and their impact on GNSS signals [10]–[12]. Furthermore, radio-occultation (RO) experiments onboard missions such as FORMOSAT-7/COSMIC-2 (F7/C2) [13] extend the coverage of observations to include regions with no established scintillation monitoring networks. This work proposes scaling widely available GNSS L-band amplitude-scintillation observations to D2C frequencies to assess scintillation risk to D2C links as a function of local time, season, signal

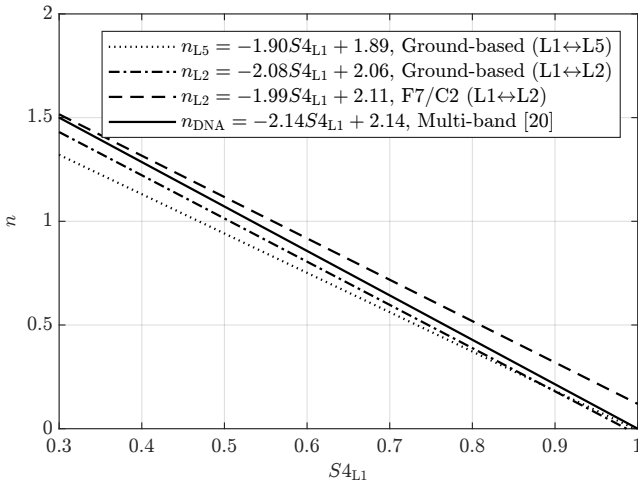


Fig. 1. frequency exponent  $n$  versus  $S4_{L1}$ .

TABLE I

Performance metrics of the LS best-fit and DNA

Scaling	LS best-fit		DNA	
	RMSE	$R^2$	RMSE	$R^2$
L1 to L5	0.085	0.76	0.086	0.76
L1 to L2 (Ground-based)	0.074	0.82	0.074	0.82
L1 to L2 (F7/C2)	0.087	0.72	0.085	0.73

arrival direction, and solar activity. Here, we provide a proof of concept on how this can be achieved by using data from a multi-frequency GNSS reference receiver located at Sharjah, United Arab Emirates. Furthermore, the ground-based observations are compared to space-based RO amplitude scintillation observations from F7/C2 to gauge the suitability of using space-based RO observations in regions that lack ground-based scintillation monitoring receivers.

The scaling of ionospheric scintillation from one frequency to another was investigated previously. For instance, L-band scintillation was scaled to very high frequency (VHF) in [14], and the different GNSS L-band frequencies (L1/L2/L5) in [15], [16]. Furthermore, using GNSS L-band scintillation observations as a proxy model for scintillation at UHF was presented in [17]. Yet, what is missing from the literature is a self-contained long-term study on the scaling of scintillation from L-band to D2C frequencies, including comparisons with space-based RO measurements, and the conclusions that can be derived as a result.

## II. METHODOLOGY

In this work, we utilize GNSS Ionospheric scintillation observations to assess how D2C signals might be affected. We rely on a PolaRx5S multi-frequency multi-constellation reference GNSS receiver located at Sharjah (Geographic Latitude:  $25.28^\circ$ , Geographic Longitude:  $55.46^\circ$ ), United Arab Emirates, which provides data over the ascending phase of solar cycle 25 (2020–2024). The

retrieved observations correspond to L1 scintillation from GPS L1 C/A and Galileo E1, both having a carrier frequency of 1575.42 MHz. Additionally, to limit the influence of multipath on scintillation, this work utilizes observations with an elevation greater than  $30^\circ$ .

This work also utilizes RO amplitude scintillation observations from F7/C2 for the years 2023–2024<sup>1</sup>. The longitude and latitude values of the observations were limited to  $54^\circ \leq \text{longitude} \leq 57^\circ$  and  $23^\circ \leq \text{latitude} \leq 27^\circ$  to enable a comparison with observations from the ground-based receiver by matching the region of coverage. Additionally, only GPS observations were used in this work for F7/C2.

Amplitude scintillation is represented by the standard deviation of the signal's intensity ( $I$ ) normalized to the average signal intensity over 60 seconds [18], i.e.,

$$S4 = \sqrt{\frac{\langle I^2 \rangle - \langle I \rangle^2}{\langle I \rangle^2}}. \quad (1)$$

The severity of scintillation can be inferred from the magnitude of  $S4$ , where weak, moderate, and strong scintillation are represented by  $S4 < 0.3$ ,  $0.3 \leq S4 \leq 0.6$ , and  $S4 > 0.6$ , respectively [18]. This work focuses on strong scintillation, since such events can cause peak-to-peak power fluctuations greater than 14 dB [6].

To translate the scintillation occurrences seen at L-band GNSS signals to those that could be seen at D2C signals, we use the standard frequency scaling relation [18]

$$S4_{f_2} = S4_{f_1} \left( \frac{f_2}{f_1} \right)^{-n}, \quad (2)$$

where  $S4_{f_1}$  is the S4 observation at frequency  $f_1$ , and  $S4_{f_2}$  is the scaled S4 at frequency  $f_2$ . Furthermore, the frequency exponent  $n$ , which characterizes the signal frequency dependence of amplitude scintillation [14], is represented by

$$n = \frac{\ln \left( \frac{S4_{f_2}}{S4_{f_1}} \right)}{\ln \left( \frac{f_1}{f_2} \right)}. \quad (3)$$

The frequency scaling exponent  $n$  for frequencies ranging from 30 MHz to 6 GHz, as observed from multiple satellite measurements, was found to range between 1 to 2 (see Table 3.4 in [19]). Of these different experiments, the observations taken by the Defense Nuclear Agency (DNA) wideband satellite experiment were the most prolific. The DNA satellite acted as a multi-frequency coherent radio beacon targeted towards studying the ionospheric scintillation of signals in the VHF, UHF, L, and S-bands. Through its observations, the value  $n = 1.5$  was empirically derived [20] for the weak scattering assumption, i.e., weak to moderate scintillation [18], [19]. As the magnitude of  $S4$  increases and approaches unity,  $n$  saturates at 0 [18], [20]. Therefore, the trend of  $n$

<sup>1</sup>The first available scintillation observation from F7/C2 was in 25/03/2022. Observations of the year 2022 were omitted to focus on complete years.

TABLE II  
Bands of D2C signals

Band	UL Freq. (MHz)	DL Freq. (MHz)	Ref.
Low-band (AST and AT&T)	698–849	728–894	[21]
PCS G Block (Starlink and T-Mobile)	1910–1915	1990–1995	[22]
NR N255	1626–1660	1525–1559	[23]
NR N256	1980–2010	2170–2200	[23]

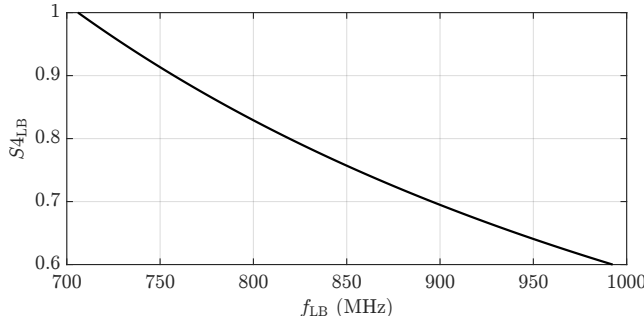


Fig. 2.  $S4_{LB}$  values corresponding to  $S4_{L1} = 0.3$ .

can be well represented by a linear relationship between moderate and strong values of scintillation, where  $n = 1.5$  at  $S4 = 0.3$  and  $n = 0$  at  $S4 = 1$  [14].

To see if this DNA-derived linear trend is applicable in our scenario, five years of simultaneous observations of GPS-derived  $S4_{L1}/S4_{L2}/S4_{L5}$  from the ground-based receiver and two years of simultaneous observations of  $S4_{L1}/S4_{L2}$  from F7/C2 were used, with the value of  $n$  calculated as in (3) for  $0.3 \leq S4 \leq 1$ . Next, a least-squares approach was utilized to obtain the best-fit line for  $n_{L2}$  that scales  $S4_{L1}$  to  $S4_{L2}$ , and  $n_{L5}$  that scales  $S4_{L1}$  to  $S4_{L5}$ . The least-squares best fit equations for each case are presented in Fig. 1. Note that the reverse procedure, e.g., scintillation observed at L5 scaled to L1 instead, would yield similar results to L1 scintillation scaled to L5.

In Fig. 1, the solid line represents the  $n_{DNA}$  proposed by [20], and as can be seen it is very close in magnitude to our empirically derived ground-based and F7/C2  $n_{L2}$  and  $n_{L5}$ , indicating the suitability of the DNA-derived  $n_{DNA}$  values. Since  $n_{DNA}$  was derived from multi-band observations, it will be used in this work to scale S4 from GNSS to D2C frequencies. To evaluate the performance consequences of this choice, the  $n_{L2}$  and  $n_{L5}$  were used to scale scintillation observed on L1 to L2 and L5, respectively. Then,  $n_{DNA}$  was used to perform the same procedure. The scaled scintillation values were then compared to the true observed L2/L5 values, and the errors in terms of RMSE and  $R^2$  are provided in Table I. As can be seen from Table I, the performance metrics almost match, which proves the suitability of using  $n_{DNA}$  to scale scintillation from GNSS to D2C frequencies.

D2C communication would be performed in two ways. Spectrum sharing between telecommunication and

TABLE III  
Number of strong scintillation observations

Band	Number of $S4 > 0.6$ observations	
	Ground-based	F7/C2
L1	9 652	1 460
Low-band	25 875	5 275
NR N255	9 447	1 409
NR N256	7 432	982

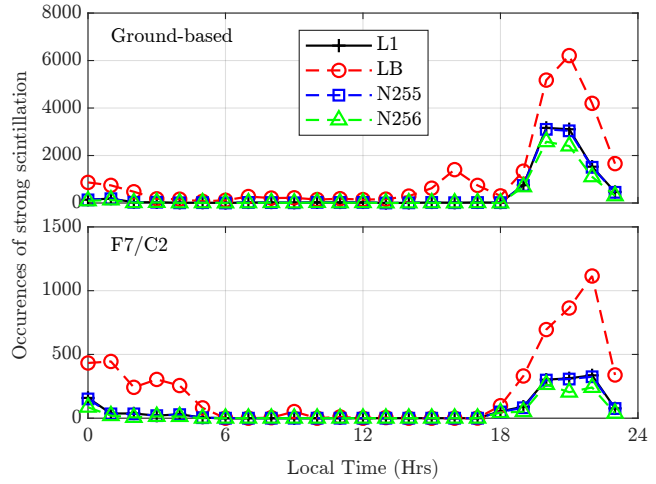


Fig. 3. Hourly trend of strong scintillation occurrences.

satellite companies, such as AST SpaceMobile with AT&T or Starlink and T-Mobile, or using new spectrum such as NR N255 and N256 introduced by the 3GPP Standard Release 17 (see Table II for details). Due to the frequency dependence of scintillation, the low-band is particularly prone to ionospheric scintillation as can be seen in Fig. 2, where moderate scintillation seen in L1 ( $S4 = 0.3$ ) equals strong scintillation ( $S4 > 0.6$ ) in the low-band.

This work will focus on three bands by scaling the L1 scintillation to three distinct frequencies: N255 represented by 1600 MHz, N256 represented by 2000 MHz (this also covers PCS G Block due to similar frequency values), and low-band represented by 800 MHz.

### III. OBSERVATIONS

After scaling the L1 scintillation to the three distinct frequencies, Figs. 3–6 were plotted to assess the spatial and temporal characteristics of scintillation at D2C frequencies. These trends represent the number of minute-by-minute occurrences (or observations) of strong scintillation.

Over the entire study period (Table III), the number of scintillation observations in the low-band was  $2.68 \times$  and  $3.61 \times$  those observed at L1 from ground-based and F7/C2 measurements, respectively. In contrast, the occurrence rates at N255 were comparable to L1, at approximately  $0.98 \times$  and  $0.97 \times$  of the L1 ground-based and F7/C2 observations. For N256, the corresponding occurrences

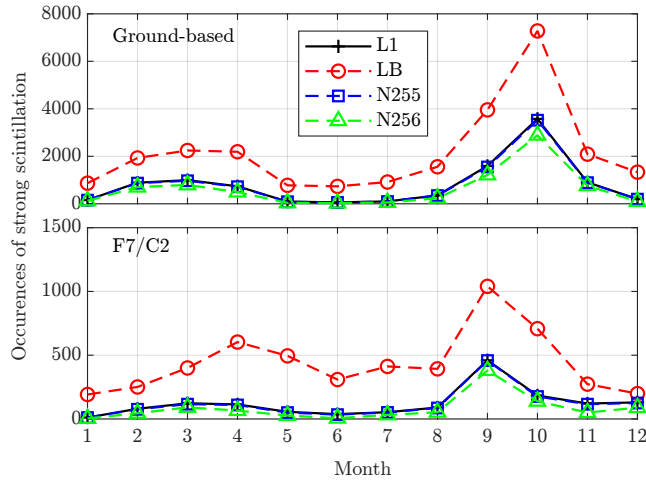


Fig. 4. Monthly trend of strong scintillation occurrences.

were lower, at  $0.77\times$  and  $0.67\times$  of the L1 ground-based and F7/C2 observations, respectively.

Fig. 3 shows the diurnal variation of scintillation. The solid line represents the L1 strong scintillation observations, while the circle markers represent the low-band observations, followed by N255 and N256, represented by the square and triangle markers respectively.

The largest peak of scintillation as observed by F7/C2 and the ground-based receiver is seen at 20–22 local time for all bands, corresponding to the post-sunset to midnight period. A second minor peak is also seen by the ground-based receiver at the low-band at 15–17 local time which represents the pre-sunset period. This secondary peak is typically observed from weak L-band scintillation [24], but due to the frequency dependence of scintillation, this weak scintillation at L-band is translated to strong scintillation in the low-band [17]. Another peak is observed after the midnight period by both instruments, with F7/C2 observing it for a more extended period up to 6 hours.

The number of strong scintillation occurrences at the low-band at its peak is more than double the peak of N255 and N256 as observed by ground and space-based instruments, which highlights the challenge to be faced by low-band D2C systems. Fig. 3 also shows that even N256 with its higher frequency will be subjected to considerable levels of strong scintillation.

Fig. 4 shows the seasonal variation of scintillation. For all trends, the summer and winter seasons saw the lowest number of scintillation observations, while the equinoxes, and particularly the autumnal equinox (September–October), had the highest occurrence of scintillation, for both ground and space-based instruments. This period coincides with the solar terminator being parallel to the geomagnetic field [25]. Similar to Fig. 3, the occurrence peaks for low-band during the equinoxes are more than twice that for N255 and N256.

Fig. 5 shows the yearly variation of scintillation, which shows the impact of solar activity. Additionally, Fig. 5 (lower) shows the solar radio flux at 10.7 cm in

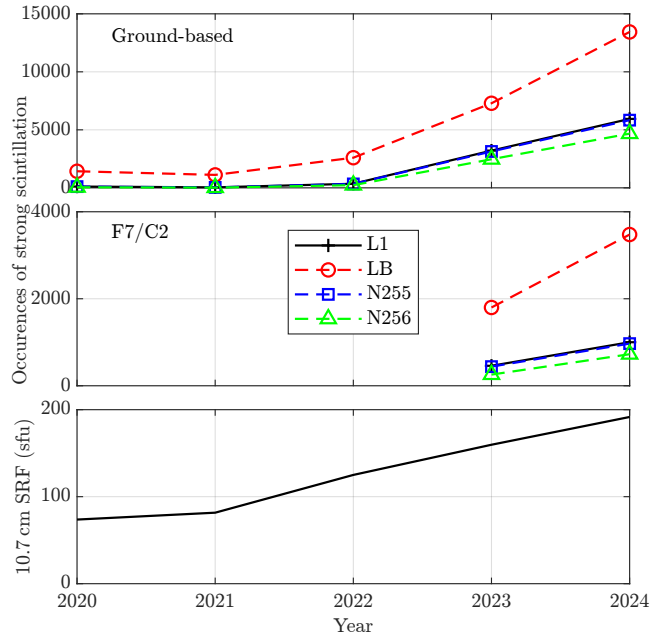


Fig. 5. Yearly trend of strong scintillation occurrences. Lower plot: F10.7 solar radio flux in sfu.

solar flux units (sfu)<sup>2</sup>, which is used as an indicator for solar activity. The sun undergoes an 11 year cycle of activity, and the peak of the current solar cycle (cycle 25) was in 2024 [26]. Therefore, observing the increase in strong scintillation from the solar cycle minimum in 2020 to its peak in 2024 allows us to understand how solar activity impacts the number of strong scintillation events at different D2C frequencies.

Each trend shows similar values in 2020 and 2021 followed by a gradual increase in 2022 and a sharp increase in 2023 and 2024. This increase is also reflected in the F7/C2 observations. Similar to Figs. 3–4, the number of low-band strong scintillation occurrences is more than twice the other bands.

Fig. 6 shows the spatial distribution of scintillation, with each subplot representing a different band. The number of strong scintillation occurrences is represented by the radial axis, while the azimuth is represented by the angular axis with a resolution of  $30^\circ$ .

All subplots show that the majority of strong scintillation is seen from the south. In fact, the percentage of northerly occurrences was 23% for low-band, and 7% and 5% for N255 and N256, respectively. This shows that almost all strong scintillation is induced on N255 and N256 links from the south, while almost three-quarters of all strong observations on low-band are from the south. This is due to scintillation effects being more intense nearer to the equator than high latitude regions [27].

Studying the spatial and temporal characteristics of ionospheric scintillation at D2C frequencies for different

<sup>2</sup>The data was obtained from the GSFC/SPDF OMNIWeb interface at <https://omniweb.gsfc.nasa.gov>

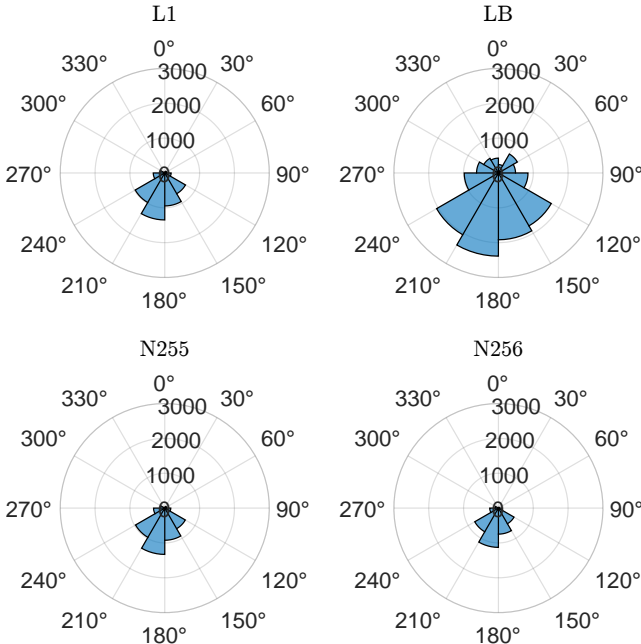


Fig. 6. Azimuth of strong scintillation occurrences.

regions is essential for assessing link robustness and planning operational strategies. For example, temporal patterns help identify periods in which the user-satellite links are more likely to degrade, enabling operators to schedule adaptive mitigation techniques [8]. Spatial patterns, particularly the strong southerly azimuth dependence observed in this region, enable operators to enact strategies that prioritize geometries less affected by scintillation. For example, since D2C constellations are large, higher weights can be assigned to northern communication links during periods of anticipated strong scintillation. Having these insights allows D2C system operators to anticipate performance degradation rather than react to it, which improves the quality of service of D2C systems.

#### IV. CONCLUSION

This work demonstrated the use of scaled GNSS-frequency scintillation observations to characterize the spatial and temporal variability of amplitude scintillation at D2C frequencies. As a case study, five years of ground-based data from a GNSS receiver in Sharjah, United Arab Emirates, together with two years of space-based observations from the F7/C2 mission over the same region, were analyzed. Both datasets revealed a pronounced diurnal peak between 20–22 local time, with scintillation occurrences concentrated around the equinoxes and increasing with solar activity. Ground-based observations further indicated a clear azimuth dependence, with the majority of strong scintillation occurrences associated with southward satellite links. These results demonstrate that scaled GNSS scintillation observations can serve as

a key indicator of scintillation risk for D2C link reliability. Future work will focus on validating these findings using measurements from D2C ground-based monitoring stations and satellite-derived signal quality metrics.

#### REFERENCES

- [1] M. A. Jamshed, A. Kaushik, M. Dajer, A. Guidotti, F. Parzysz, E. Lagunas, M. Di Renzo, S. Chatzinotas, and O. A. Dobre, “Non-terrestrial networks for 6G: Integrated, intelligent, and ubiquitous connectivity,” *IEEE Communications Standards Magazine*, vol. 9, no. 3, pp. 86–93, 2025.
- [2] J. G. Andrews, T. E. Humphreys, and T. Ji, “6G takes shape,” *IEEE BITS the Information Theory Magazine*, vol. 4, no. 1, pp. 2–24, 2024.
- [3] A. K. Sun, S. Pullen, and J. Lee, “Analysis of diffraction-induced residual errors in GNSS augmentation systems under ionospheric scintillation,” *IEEE Transactions on Aerospace and Electronic Systems*, pp. 1–10, 2025.
- [4] L. Marini-Pereira, A. de Oliveira Moraes, and S. Pullen, “Advanced warning of threatening equatorial plasma bubbles to support GBAS in low latitudes,” *IEEE Transactions on Aerospace and Electronic Systems*, vol. 59, no. 5, pp. 4858–4869, 2023.
- [5] E. Pica, A. Minetto, C. Cesaroni, and F. Dovis, “Analysis and characterization of an unclassified RFI affecting ionospheric amplitude scintillation index over the mediterranean area,” *IEEE Journal of Selected Topics in Applied Earth Observations and Remote Sensing*, vol. 16, pp. 8230–8248, 2023.
- [6] ITU, “Ionospheric propagation data and prediction methods required for the design of satellite networks and systems,” International Telecommunication Union, Tech. Rep. Recommendation ITU-R P.531-16, 09 2025.
- [7] C. R. Aguiar, J. F. G. Monico, and A. O. Moraes, “Impact of ionospheric scintillations on GNSS availability and precise positioning,” *Space Weather*, vol. 23, no. 2, p. e2024SW004217, 2025.
- [8] J. Vilà-Valls, P. Closas, C. Fernández-Prades, and J. T. Curran, “On the mitigation of ionospheric scintillation in advanced GNSS receivers,” *IEEE Transactions on Aerospace and Electronic Systems*, vol. 54, no. 4, pp. 1692–1708, 2018.
- [9] J. Garcia-Cabeza, J. Albert-Smet, Z. Frias, L. Mendo, S. A. Azcoitia, and E. Yraola, “Direct-to-cell: A first look into Starlink’s direct satellite-to-device radio access network through crowdsourced measurements,” 2025. [Online]. Available: <https://arxiv.org/abs/2506.00283>
- [10] A. Dodson, T. Moore, M. H. Aquino, and S. Waugh, “Ionospheric scintillation monitoring in northern Europe,” in *Proceedings of the 14th International Technical Meeting of the Satellite Division of The Institute of Navigation (ION GPS 2001)*, 2001, pp. 2490–2498.
- [11] P. T. Jayachandran, R. B. Langley, J. W. MacDougall, S. C. Mushini, D. Pokhotelov, A. M. Hamza, I. R. Mann, D. K. Milling, Z. C. Kale, R. Chadwick, T. Kelly, D. W. Danskin, and C. S. Carrano, “Canadian high arctic ionospheric network (CHAIN),” *Radio Science*, vol. 44, no. 01, pp. 1–10, 2009.
- [12] B. C. Vani, A. de Oliveira Moraes, L. A. Salles, V. H. Fernandes Breder, M. José dos Santos Freitas, J. F. Galera Monico, and E. Rodrigues de Paula, “Chapter 13 - Monitoring ionospheric scintillations with GNSS in South America: scope, results, and challenges,” in *GPS and GNSS Technology in Geosciences*, G. p. Petropoulos and P. K. Srivastava, Eds. Elsevier, 2021, pp. 255–280.
- [13] X. Yue, W. S. Schreiner, N. Pedatella, R. A. Anthes, A. J. Mannucci, P. R. Straus, and J.-Y. Liu, “Space weather observations by GNSS radio occultation: From FORMOSAT-3/COSMIC to FORMOSAT-7/COSMIC-2,” *Space Weather*, vol. 12, no. 11, pp. 616–621, 2014.
- [14] A. Bhattacharyya, P. Gurram, B. Kakad, S. Sripathi, and S. Sunda, “Signal frequency dependence of ionospheric scintillations: An

indicator of irregularity spectrum characteristics," *Journal of Geophysical Research: Space Physics*, vol. 124, no. 10, pp. 8081–8091, 2019.

[15] K. Song, K. Meziane, A. Kashcheyev, and P. T. Jayachandran, "Multifrequency observation of high latitude scintillation: A comparison with the phase screen model," *IEEE Transactions on Geoscience and Remote Sensing*, vol. 60, pp. 1–9, 2022.

[16] C. S. Carrano, K. M. Groves, S. H. Delay, and P. H. Doherty, "An inverse diffraction technique for scaling measurements of ionospheric scintillations on the GPS L1, L2, and L5 carriers to other frequencies," in *Proceedings of the 2014 international technical meeting of the institute of navigation*, 2014, pp. 709–719.

[17] R. G. Caton, W. J. McNeil, K. M. Groves, and S. Basu, "GPS proxy model for real-time UHF satellite communications scintillation maps from the scintillation network decision aid (SCINDA)," *Radio Science*, vol. 39, no. 1, pp. 1–8, 2004.

[18] 3GPP, "Study on New Radio (NR) to support non-terrestrial networks," 3rd Generation Partnership Project (3GPP), Tech. Rep. 38.811, 09 2020, version 15.4.0.

[19] A. D. Wheelon, *Electromagnetic scintillation: volume 2, weak scattering*. Cambridge University Press, 2006.

[20] E. J. Fremouw, R. L. Leadabrand, R. C. Livingston, M. D. Cousins, C. L. Rino, B. C. Fair, and R. A. Long, "Early results from the DNA wideband satellite experiment—complex-signal scintillation," *Radio Science*, vol. 13, no. 1, pp. 167–187, 1978.

[21] FCC, Federal Communications Commission, Tech. Rep. DA 25-815, 9 2025.

[22] ——, Federal Communications Commission, Tech. Rep. DA 24-1193, 11 2024.

[23] 3GPP, "Satellite access node radio transmission and reception," 3rd Generation Partnership Project (3GPP), Tech. Rep. 38.108, 01 2024, version 17.6.0.

[24] A. M. Darya, M. M. Shaikh, G. Nykiel, E. Ghamry, and I. Ferrini, "Multi-instrument analysis of L-band amplitude scintillation observed over the eastern Arabian Peninsula," *Advances in Space Research*, vol. 74, no. 4, pp. 1856–1867, 2024.

[25] Y. Otsuka, "Review of the generation mechanisms of post-midnight irregularities in the equatorial and low-latitude ionosphere," *Progress in Earth and Planetary Science*, vol. 5, no. 1, p. 57, 2018.

[26] B. K. Jha and L. A. Upton, "Predicting the timing of the solar cycle 25 polar field reversal," *The Astrophysical Journal Letters*, vol. 962, no. 1, p. L15, Feb 2024.

[27] Y. Jiao, D. Xu, C. L. Rino, Y. T. Morton, and C. S. Carrano, "A multifrequency GPS signal strong equatorial ionospheric scintillation simulator: Algorithm, performance, and characterization," *IEEE Transactions on Aerospace and Electronic Systems*, vol. 54, no. 4, pp. 1947–1965, 2018.